EUROfusion

EUROFUSION CP(15)05/17

V.T. Tikhonchuk et al.

Physics of Laser-Plasma Interaction and Shock Ignition of Fusion Reactions

(22nd June 2015 – 26th June 2015)
Lisbon, Portugal

This work has been carried out within the framework of the EUROfusion Consortium and has received funding from the Euratom research and training programme 2014-2018 under grant agreement No 633053. The views and opinions expressed herein do not necessarily reflect those of the European Commission.

Physics of Laser-Plasma Interaction and Shock Ignition of Fusion Reactions

V. T. Tikhonchuk[1], A. Colaïtis[1], A. Vallet[1,2], E. Llor Aisa[1], G. Duchateau[1], Ph. Nicolaï[1], X. Ribeyre[1]

[1] University of Bordeaux - CEA - CNRS, Centre Lasers Intenses et Applications, UMR 5107, 33405 Talence Cedex, France

[2] CEA, DAM, DIF, F-91297 Arpajon, France

E-mail: tikhonchuk@celia.u-bordeaux1.fr

Abstract. The Shock Ignition scheme is an alternative approach, which aims to achieve ignition of fusion reactions in two subsequent steps: first, the target is compressed at a low implosion velocity and second, a strong converging shock launched during the stagnation phase ignites the hot spot. In this paper we describe the major elements of this scheme and recent achievements concerning the laser-plasma interaction, the crucial role of hot electrons in the shock generation, the shock amplification in the imploding shell and the ignition conditions.

PACS numbers: 52.35.Mw, 52.38.Bv, 52.38.Kd, 52.65.Rr

Submitted to: *Plasma Phys. Control. Fusion*

1. Introduction

Inertial confinement fusion (ICF) approaches a major turning point in its history with a unique opportunity offered by two megajoule laser facilities, NIF in the USA and LMJ in France, for testing the ignition schemes on a full scale. The indirect ignition scheme, already tested on the NIF [1], is considered to be more stable and robust, but it is less efficient, the targets are too complicated in fabrication and too heavy for using in energy production schemes. Here, the spherical shell containing the ablator and fuel is imploded by the intense X-ray radiation, which is created at the internal surface of a heavy cavity irradiated by laser. The ignition occurs in the central hot spot providing a spark for combustion of the main part of fuel. However, not all background physical processes are well understood and correctly modeled, so the ignition conditions are not yet achieved.

The energy production requires a more efficient ignition scheme, a technologically feasible target with a sufficiently large fraction of fuel in the total target mass and a high repetition high energy laser system. While the multi-shot operation is still awaiting the major breakthrough in the laser technology, the target ignition should be demonstrated on the existing laser facilities, which deliver a sufficient energy and a flexible pulse shape. The standard direct drive scheme indeed relies on a direct laser irradiation of simple spherical targets containing about 50% of fuel. However, it requires too much laser energy essentially because both megajoule laser facilities are conceived for the indirect drive and cannot provide a fully symmetric target irradiation.

The Shock Ignition (SI) scheme [2, 3, 4] is an alternative direct drive ICF approach, which proposes to achieve ignition in two subsequent steps: first, the target is compressed at a low implosion velocity, less than 300 km/s, and then a strong converging shock is launched during the stagnation phase to ignite the hot spot. The low velocity implosion requires a relatively modest laser energy, about $200 - 400$ kJ, and makes the target more hydrodynamically stable. The energy needed for the hot spot ignition, about $200 - 300$ kJ, is brought with a strong shock driven by a separate intense laser spike. The preliminary studies of the Shock Ignition scheme [5, 6] show that it can be tested on a full scale on the NIF and LMJ facilities. It is chosen as a baseline in the European ESFRI project HIPER for the inertial confinement energy production [7].

These relatively low energy requirements for the SI scheme have to be considered with caution as the physics included in the simulation codes is limited to basic hydrodynamic effects and to a simplified description of the laser plasma interaction processes. While it may be sufficient during the imploding phase, where the laser power is relatively low, it is definitely insufficient for the laser spike of a high intensity, where the effects of nonlinear laser plasma interaction and kinetic transport become dominant. In this paper we present the major achievements in the understanding of the shock ignition physics. This concerns the laser-plasma interaction, demonstration of the crucial role of hot electrons in the shock generation, shock pressure amplification in the imploding shell and the ignition criterion.

The paper contains three parts. The conditions of fuel ignition by a strong shock are considered in Sec. 2. These conditions are defining the strength of shock that needs to be excited with a laser spike. The required ablation pressure is in the range of $300-500$ Mbar. Only recently such an extremely high pressure has been demonstrated in a multi beam irradiation of a spherical target on the Omega facility [8] at laser intensities approaching 10 PW/cm^2. At such intensities the physics of laser plasma interaction is strongly nonlinear, and generation of high ablation pressures is related to energy deposition in a compressed shell by a flux of energetic electrons. The model of high intensity laser plasma coupling and strong shock generation is considered in Sec. 3 followed by presentation of the integrated model for the shock ignition target design in Sec. 4.

2. Fuel ignition with a strong shock wave

Let us first recall the necessary conditions of the fuel ignition with a strong spherical shock. The laser pulse shape and shell trajectory are shown in figure 1. At the beginning of implosion, the laser radiation ablates the outer layer of a spherical target. A pressure created at the ablation front produces a shock propagating through the shell. The laser pulse intensity increases slowly generating a sequence of compression waves, which merge with the primary shock at the inner side of the shell (zone 1 in figure 1). The shock is transmitted partially into the deuterium-tritium (DT) gas and a rarefaction wave is reflected into the shell. This sequence of processes starts the acceleration phase of the shell. In the same time, the shock in the DT gas converges and reflects at the center of the target. The acceleration phase is ended when the diverging primary shock collides with the shell (zone 2). At this time the shell attains its maximum velocity $u_{\rm imp}$ and starts to decelerate due to the increasing pressure in the compressed DT gas. The stagnation phase achieved when the shell velocity comes to zero is the most appropriate moment for ignition of the fuel in the standard ICF scheme. However, in the shock ignition scheme, the shell implosion velocity is not sufficient to raise the DT gas temperature to ignition conditions. An additional energy is brought with the ignitor shock (zone 3 in figure 1). It is launched during the acceleration phase in such a way that it collides with the reflected primary shock (zone 4), enters into the fuel (zone 5) and increases the fuel temperature above the ignition threshold.

The major challenge of the shock ignition scheme is defining the strength of the ignitor shock and the time when it should be launched. An analytical approach presented below allows to consider the underlying physical mechanisms. It follows by the optimization stage performed with extended numerical simulations. We start from the ignition conditions and then will go back in time estimating the shock evolution as it propagates through the shell. Let assume that the ignitor shock having velocity U_{s0} enters in the DT gas with the density ρ_0 at the moment t_0 when shell inner radius is R_0. The shell acts a piston launching the shock in a gas. Neglecting the initial gas pressure, the propagation of a strong shock is described by the self-similar solution by Guderley

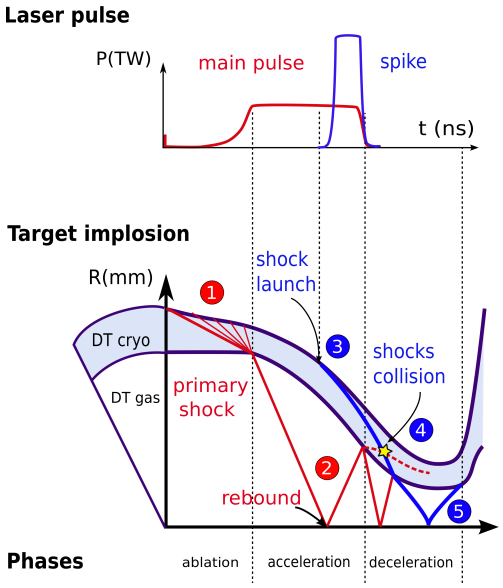

Figure 1. Synopsis of the laser pulse shape and the target implosion in the shock ignition scheme.

[9]. The collapse time t_c is defined by the relation $t_c - t_0 = \alpha R_0/U_{s0}$, where $\alpha \simeq 0.688$ is the parameter in the self-similar variable $\xi = r/|t - t_c|^\alpha$. At the converging phase the gas compression increases from the factor of 4 as in a planar strong shock to 9.5 at the moment of collapse. The density behind the outgoing shock is further increased as it propagates through the hot spot. As it emerges at the shell boundary, the fuel is compressed by a factor 32.28 with respect to the initial gas density and the pressure is increased by a factor of 40.

The shock exit time $t_{\rm ex} = t_c + 0.324\alpha R_0/U_{s0}$ is the most appropriate time for the fuel ignition as it corresponds to the maximum areal fuel density and the maximum temperature. A criterion for fusion ignition in the hot spot has been evaluated in Ref. [10] from the balance of the power released in the DT fusion reactions and the power losses due to the electron heat conductivity, radiation and escaping α-particles and neutrons. The shock velocity required for ignition is shown in figure 2a in function of the DT gas areal density $\rho_0 R_0$ with dashed lines. The minimum shock velocity is about 600 km/s and the minimum areal density is 15 mg/cm^2. To obtain this criterion, it is important to account for the appropriate temperature dependence of the rate of fusion reactions and for the α-particle losses from the hot spot.

The self-similar solution underestimates the ignition threshold because of neglecting the initial DT gas pressure. The hot spot is, however, heated after the primary shock is reflected from the center (see zone 2 in figure 1). The numerical simulations show that the DT gas can be heated to a temperature about 1 keV, which corresponds to the shell effective Mach number $M_{s0} = U_{s0}/c_s = 2 - 4$. The effect of the finite gas sound velocity c_s on the ignition threshold was considered in Ref. [11] by using a perturbative approach

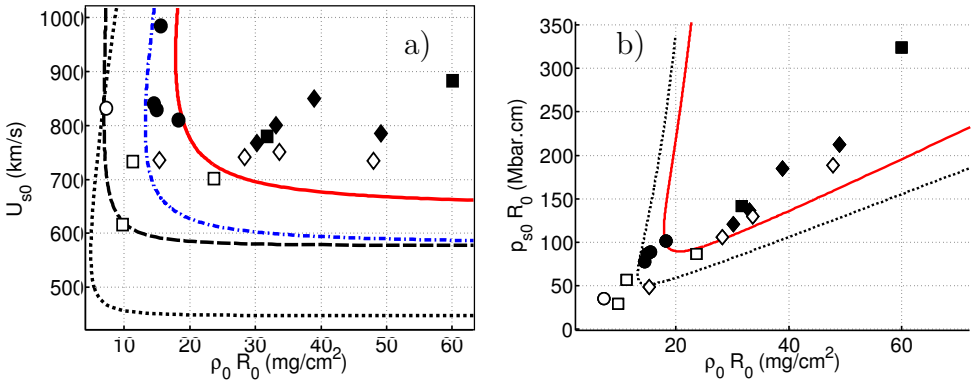

Figure 2. Shock ignition threshold in function of the initial gas areal density. a) Dependence of the initial shock velocity: dashed lines – infinite shock strength with (blue) and without (black) α-particle losses. Dotted black line corresponds to a simplified T^2 dependence of the DT reaction rate on the temperature. Red line – the shock Mach number $M_{s0} = 4$. b) Dependence of the initial shock pressure for the infinite (dotted) and $M_{s0} = 4$ (red) shock strength. Symbols present the results of hydrodynamic simulations with the standard HiPER target for the cases where ignition was achieved (closed symbols) and without ignition (open symbols).

over a small parameter $M_{s0}^{-2} \ll 1$. The correction affects mainly the gas density and the pressure after the shock rebound. Correspondingly, the shock ignition threshold is modified by more than 20% for $M_{s0} = 4$. As can be seen in figure 2a, the shock ignition velocity increases to more than 700 km/s and the minimum areal density rises to 18 mg/cm^2. This increase of the ignition threshold is explained by a less efficient fuel heating in a small amplitude shock.

These analytical predictions are confirmed in the hydrodynamic simulations of ignition of a standard HiPER target [4] described below. The closed symbols in figure 2a show the cases where the fuel was ignited. It is also instructive to express the ignition threshold in function of the shock pressure according to the relation $p_{s0} \propto \rho_0 U_{s0}^2$, as it is shown in figure 2b. For example, for the inner shell radius $R_0 = 50\,\mu$m the ignition condition corresponds to the gas density $\rho_0 = 4$ g/cm^3, the pressure $p_{s0} = 20 - 30$ Gbar and the initial shock velocity in the hot spot $U_{s0} = 700$ km/s. Generate such a shock pressure is very challenging. It cannot be achieved directly in the ablation zone, thus the amplification of the shock pressure in the imploding shell is a key element for shock ignition.

The converging shock description considered above applies for an initial gas of a constant density at rest. The shock propagation through an imploding shell requires a special analysis as the shell is accelerated and its density and pressure are inhomogeneous. According to the results obtained in Ref. [12], the overall shock amplification in the imploding shell can be represented as a product of three factors: the shell pressure amplification as it implodes, $\chi_{\rm imp}$, the shock amplification as it crosses

the shell, $\chi_{\rm shell}$, and the shock amplification in the collision with the returning primary shock $\chi_{\rm coll}$. Thus the overall shock pressure amplification factor reads:

$$p_{sf}/p_{si} = \chi = \chi_{\rm imp}\chi_{\rm shell}\chi_{\rm coll}. \quad (1)$$

Assuming a self-similar shell implosion with the polytrope parameter $\gamma = 5/3$, its radius is proportional the scale factor, $R \propto h(t)$, the density scales as h^3 and the pressure scales as h^5. Thus the shell pressure amplification factor is $\chi_{\rm imp} = (h(t_i)/h(t_f))^5$. It may achieve the values of $\chi_{\rm imp} \sim 15 - 20$ during the time ~ 300 ps of shock crossing the shell.

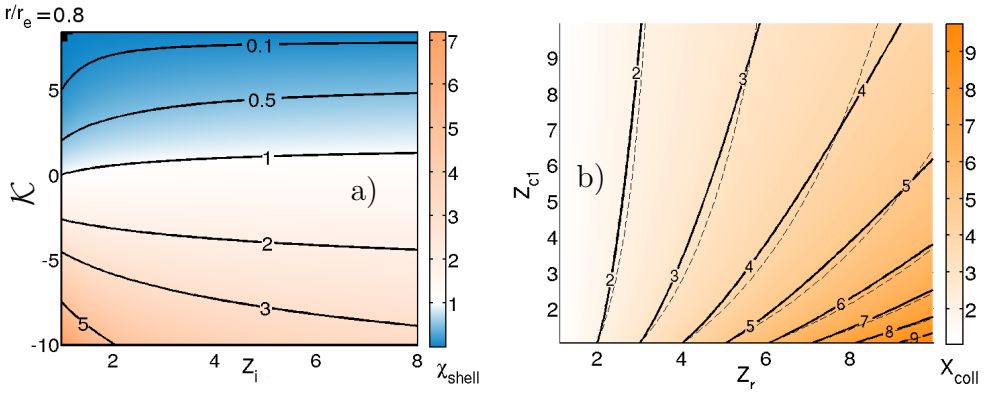

Figure 3. a) Dependence of the shock pressure amplification factor in the shell reference frame $\chi_{\rm shell}$ on the initial shock strength Z_i and the shell density gradient $\mathcal{K}$. b) Dependence of the shock pressure amplification factor in the shock collision $\chi_{\rm coll}$ on the strength of colliding shocks.

The shock evolution in the shell co-moving frame is studied with the so-called freely propagating shock wave approximation [13] where the influence of the downstream flow on the shock dynamics is neglected. Then the shock strength Z, which is the ratio of downstream to upstream pressures, $Z = p^{\rm down}/p^{\rm up}$, depends on the upstream pressure and the density gradient. In the accelerating shell the density gradient is positive, and shock propagates in the direction of decreasing density and pressure. Hence its pressure decreases, $\chi_{\rm shell} < 1$. In contrast, in the deceleration phase the sign of density gradient is opposite, and the shock pressure is amplified. Figure 3a shows the dependence of the shock amplification factor $\chi_{\rm shell}$ in function of the initial shock strength Z_i and the dimensionless shell density gradient $\mathcal{K} = (d\rho/dr)/(\rho_{\rm in}/r_{\rm in})$ for the ratio of the shell outer and inner radii $r_{\rm out}/r_{\rm in} = 0.8$.

A collision between the ignitor and returning primary shocks is another important factor of the shock pressure amplification. As shocks propagate in opposite directions, collision converts the kinetic energy of incoming shocks into the internal energy and thus enhances the transmitted shock pressure. Assuming the both shocks to be planar, the pressure amplification factor is shown in figure 3b in function of the strengths of incoming shocks. The maximum pressure amplification is 6, if the pressures of both

shocks are equal. In the domain of interest, the pressure amplification can be presented with the following interpolation formula

$$\chi_{\rm coll} = Z_r \left(\frac{Z_c + Z_r}{1 + Z_r Z_c} \right)^{1/2} \tag{2}$$

where Z_r is the strength of returning primary shock and Z_c is the strength of the ignitor shock at the moment of collision. This approximate expression shown with the dashed lines in figure 3b agrees well with the exact solution. If the returning shock is weak, the amplification factor is about 2. For a stronger returning shock, it could be more significant.

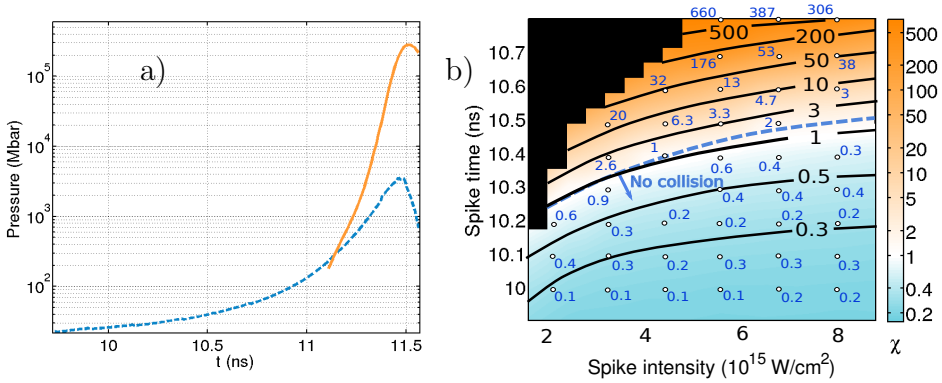

Figure 4. a) Pressure evolution in the imploding shell during the acceleration phase (dashed blue line) and deceleration phase (solid yellow line). b) Dependence of the total shock pressure amplification factor on the laser spike intensity and the launch time $t_{\rm launch}$. The case of a standard HiPER target. Open dots and blue numbers present the results obtained in hydrodynamic simulations.

As an example of shock amplification we consider the all-DT HiPER target [4] with the initial mass 0.6 mg and aspect ratio 4. The shell pressure evolution is shown in figure 4a. The total pressure amplification of the shock (1) is shown in figure 4b where the white dots represent the shock amplification measured in the hydrodynamic simulations with a laser spike. There is a good agreement between the theory and simulations results. The line $\chi = 1$ is close to the dashed line delimiting the domain where the ignitor shock undergoes a collision with the returning shock in the shell. For earlier spike times the shock propagates only in an accelerating shell. The positive pressure gradient, which compensates the acceleration force in the shell co-moving frame, induces a decrease of the shock pressure. Moreover, in this zone, the shell overall pressure is increasing slowly, which is not sufficient to compensate the shock pressure decrease in the shell co-moving frame.

For time later spike launch time $t_{\rm launch} > 10.4$ ns, the shock pressure amplification increases quickly and reaches a value of ~ 500. This rapid variation of the amplification factor up to $\chi = 50-80$ is explained by three effects: the shock collision with $\chi_{\rm coll} = 2-6$,

the shell deceleration with a sharp negative pressure gradient with $\chi_{\rm imp} \sim 2$ and a quick increase of the overall shell pressure near the stagnation time $\chi_{\rm shell} \sim 15$. The latter is due to several shocks and compression waves coming from the hot-spot and entering into the shell.

This example shows advantages of the later shock launch and the origins of the pressure amplification. With the amplification factor $\chi \sim 50 - 100$, the shock pressure of $20 - 30$ Gbar needed for ignition of the hot spot can be achieved with the ablation pressure of 300 Mbar as it was suggested in [3, 4]. However, in practice the shock cannot be launched too late. The target needs to be confined during a time long enough for the fusion reactions to ignite and for the burn wave to propagate through the fuel. So a late spike launch time results in a lower fusion gain. Moreover, the shock induced heating is less efficient if shock enters into a hot spot with a high pressure. According to the analysis of the hot spot ignition in the beginning of this section and figure 2, the ignitor shock strength or the shock Mach number need to be above $3 - 4$ to attain the ignition threshold.

3. Generation of a strong shock

The hydrodynamic analysis of the ignition conditions shows a possibility of approximately a $50 - 100$ times enhancement of the shock pressure in the imploding shell corresponding to the shock pressure in the launch zone at the level of $300 - 500$ Mbar. This is $3 - 5$ times higher than the pressure produced in the ablation zone in the conventional ICF approach. Creation of such pressures is the major challenge in the shock ignition scheme.

The required laser intensities can be readily estimated from a stationary model of laser plasma interaction. Here, the absorbed laser flux $I_{\rm L\,abs}$ is transformed near the critical density into the flux of hot electrons transporting it to the ablation surface. The injected energy flux is equilibrated by the energy flux of ejected hot vapors. Near the critical density, $\rho_{\rm cr}$, the energy balance reads: $I_{\rm L\,abs} \simeq 4\rho_{\rm cr} c_s^3$. This relation defines the plasma sound velocity, $c_s \simeq (I_{\rm L\,abs}/4\rho_{\rm cr})^{1/3}$ and the plasma pressure,

$$p_{\rm abl} \simeq \rho_{\rm cr}^{1/3} I_{\rm L\,abs}^{2/3}. \tag{3}$$

In the practical terms, for the laser wavelength of 350 nm and a DT plasma with the critical density $\rho_{\rm cr} \simeq 30$ mg/cc, the ablation pressure of 300 Mbar corresponds to the laser intensity $I_{\rm L} \simeq 8$ PW/cm^2 assuming a 50% absorption. Such an intensity is well above the thresholds of parametric instabilities, which make a strong effect on the laser propagation and energy deposition in the plasma corona.

The physics of laser plasma interaction in the conditions of shock ignition corresponding to a large, millimeter scale plasma corona and high laser intensities above 1 PW/cm^2 has been studied in numerical simulations and experiments [6]. One dimensional Particle-in-Cell (PIC) simulations [14, 15] demonstrate a change of the laser plasma interaction regime for the intensities above $1 - 3$ PW/cm^2. Instead of a

collisional absorption at lower intensities, the stimulated Raman scattering (SRS) takes over with a significant part of the laser energy transformed in a flux of energetic electrons. Although a fraction of absorbed laser energy does not change much in this transition remaining at the level of $50-70\%$, at higher intensities a significant part of absorbed energy, $\sim 60-70\%$ is transferred to a relatively small group of hot electrons with the exponential distribution in energy and a characteristic temperature $T_h = 40-80$ keV. This temperature is defined by the SRS resonance condition and does not depend on the laser intensity in the considered range of parameters, while the number of these hot electrons increases proportionally to $I_{\rm L}$.

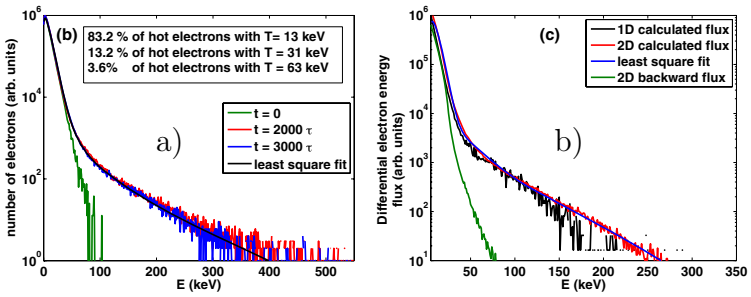

Figure 5. a) Electron distribution function in the plasma corona calculated with a PIC code and its approximation with a sum of three Maxwellian functions. b) Comparison of the differential electron energy flux obtained in one- and two-dimensional simulations. The laser intensity 8 PW/cm^2, wavelength 350 nm and the plasma scale length 300 μm. Reprinted from [17] with permission from the Institute of Physics.

These findings were confirmed in two-dimensional numerical simulations [16, 17]. Although the laser beam propagation is affected by the filamentation instability and the Two Plasmon Decay (TPD) is excited near the quarter critical density, these additional processes do not change much the overall energy balance resulting in very similar repartition of the absorbed laser energy between two dominant effects – the collisional absorption and SRS. Figure 5 shows a comparison of the electron energy flux carried in a dense plasma obtained in one- and two-dimensional simulations with the laser intensity of 8 PW/cm^2.

The experiments on the OMEGA facility are in qualitative agreement with the numerical results [18]. By using a small spherical target with the radius of 215 μm and 60 laser beams the authors have succeeded to increase the average laser intensity up to 6 PW/cm^2 with $10-12$ kJ of laser energy absorbed in the target. As it is shown in figure 6a, the hot electrons are carrying $10-20\%$ of the absorbed laser energy with the effective hot electron temperature in the range of $50-80$ keV. Moreover, the largest number of hot electrons was observed in the shots without temporal smoothing of laser beams. In this case there are large amplitude static fluctuations of the laser intensity on the target surface thus producing zones with enhanced level of parametric

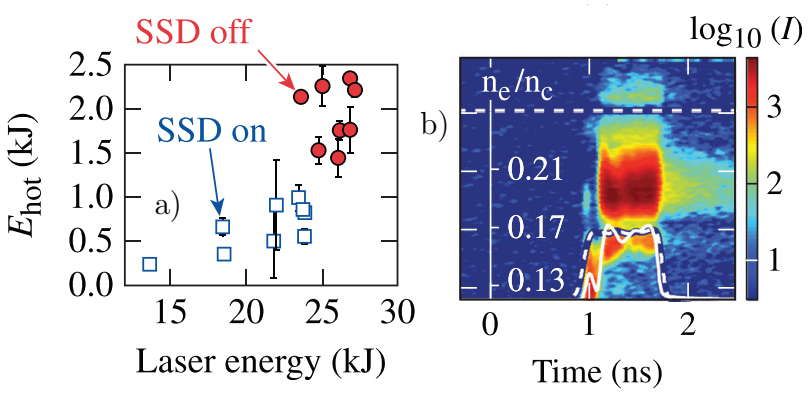

Figure 6. a) Energy fraction transmitted to hot electrons in function of the incident laser energy. The closed (red) points corresponds to the shots without laser beam temporal smoothing. b) Spectrum of the backscattered light. The vertical axis shows the plasma density where the scattered light has been produced assuming the SRS frequency matching. Temporal shapes of the incident and scattered light are shown with white solid and dashed lines, respectively. Reprinted from [18] with permission from the American Institute of Physics.

instabilities. The correlation of the hot electron generation with the SRS is confirmed by the observation of the scattered laser light with a down shift corresponding to the Raman scattering from the plasma with the densities $0.18 - 0.22$ of the critical density. These data in correlation with the observed enhanced shock amplitude indicate a significant role of hot electrons in formation of the ablation pressure.

Hot electrons are often considered as a serious obstacle for ICF as they preheat the imploding shell and decrease the accessible compression. However, the particularity of the SI scheme consists in using the main laser pulse of a lower intensity, while the strong spike arrives to the very end, when the target is already compressed and its areal density is increased to a value higher than the stopping range of hot electrons. Indeed, the initial shell areal density of 5 mg/cm^2 at the moment of the spike launch is increased by a factor of 10 to 50 mg/cm^2. This value corresponds to the stopping range of 250 keV electrons ensuring that electrons with energies below 100 keV may not compromise the shell implosion [19].

The physics of hot electron interaction with dense targets has been discussed in Ref. [20, 21]. Similarly to the laser energy deposition, the shock pressure created by energy deposition of a mono-energetic electron beam can be readily estimated from the energy balance. However, in difference from the laser-driven shock, the fast electron heating is a non-stationary process. As the stopping range of energetic electrons $R_e \propto \varepsilon^2$ depends only on the electron energy but not on the plasma parameters, the time of shock formation t_h is limited by the time of the rarefaction wave propagation across the heated region, $t_h = L_h/c_s = R_e/\rho c_s$. From these relations along with the estimate for the acoustic velocity, $c_s = (I_e/\rho)^{1/3}$, where I_e is the energy flux carried with hot

electrons, one finds an estimate for the shock pressure, $p_s \simeq \rho c_s^2 \simeq \rho^{1/3} I_e^{2/3}$. Although this expression is quite similar to (3), there are two major differences. First, the density where the electrons deposit their energy is $100-200$ times larger than the critical density, thus the same energy flux of electrons generates $5-6$ times higher shock pressure. Second, the "useful" time of electron energy deposition is proportional to the electron stopping range and it is relatively short, of the order of 100 ps. Estimates and numerical simulations show that with the electron energy flux of 1 PW/cm^2 carried out with 100 keV electrons one can achieve the pressure of more than 400 Mbar and maintain it over the time of $300-400$ ps. This corresponds quite well to the SI requirements.

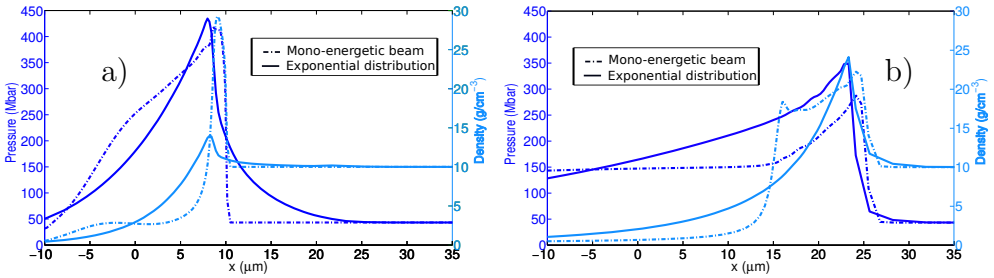

Figure 7. Shock wave formation with the mono-energetic ($\varepsilon_e = 50$ keV, dotted lines) and Maxwellian ($T_h = 25$ keV solid lines) electron beams with the energy flux 1 PW/cm^2. The DT plasma density is 10 g/cm^3. Dark blue lines – plasma pressure, light blue lines – density. Left panel: at the moment of shock formation of 90 ps. Right panel: at the time of the maximum shock strength of 250 ps.

However, there are two caveats in this reasoning that deserve a special attention [22, 23]. The first one concerns the plasma density profile. The above estimate of the shock pressure is valid for a steep density profile with a relatively thin preplasma having the areal density smaller than R_e and a thick shell with the areal density larger than R_e. A thick preplasma would reduce the maximum pressure, while a thin shell would explode if heated homogeneously. Second issue is related to the hot electron energy distribution. The reference parameter is the average electron stopping power, $\langle R_e \rangle$. For an exponential (Maxwellian) electron distribution with the temperature T_h equal to the energy of a monoenergetic electron beam, the average range is 4 times larger. Therefore, the distance and the time of shock formation are significantly increased for a Maxwellian beam. Moreover, while the shock pressure does not depend on the electron energy distribution, the shock strength is initially much weaker in the case of Maxwellian beam as it is shown in figure 7a. This fact is explained by the fast electron preheat. Although about 80% of the beam energy is deposited before the shock formation point, the remaining 20% are deposited upstream the shock thus rising the upstream pressure and reducing the shock strength. One needs to continue the electron injection during a longer time of $\sim 3t_h$ for the shock propagates the whole preheated region and regains its strength, see figure 7b. These effects demonstrate the importance of understanding

of the hot electron dynamics in the strong shock generation.

Experiments in the planar geometry so far were unsuccessful in achieving shock pressures exceeding 100 Mbar even with laser intensities of the order of 10 PW/cm^2 [6]. This is explained by a relatively low total laser pulse energy, small focal spot and, consequently, very large lateral losses. This issue was overcome in the experiments in the spherical geometry [8, 18] described above in this section. By using solid CH spheres of a radius of 215 μm and laser intensities up to 6 PW/cm^2, the authors achieved the ablation pressures up to 400 Mbar. The contribution of hot electrons was confirmed by the correlation between the shock pressure and the number of hot electrons shown in figure 6a. By removing the laser beam temporal smoothing the authors succeeded to increase the energy transferred to hot electrons up to 2 kJ followed by increased shock pressure.

This result rather important by itself, is not directly applicable to the SI conditions. A thick solid target provides an excellent environment for the shock formation. According to our simulations of that experiment [12], the maximum shock pressure is achieved at the distance more than 50 μm from the ablation surface and it is due to a complicated interplay between the shock generated by the laser pulse at the ablation surface and another shock generated by hot electrons deeper in the target.

4. Integrated model for the Shock Ignited ICF

A detailed analysis of shock ignition scheme requires good understanding of a complicated physics on multiple scales, involving laser plasma interaction and hot electron generation, hot electron transport and shock wave formation, shock wave amplification and fuel ignition. Although each of these processes can be described with a relatively simple analytical model, their mutual interaction can only be understood with an integrated model. The central part of such an integrated tool is a radiation hydrodynamics code, in our case the code CHIC [24]. It is completed with special modules describing the detailed physical processes. In application to the shock ignition scheme, the laser plasma interaction physics is of particular importance. The standard geometrical optics approach does not allow for robust evaluations of laser intensity in plasma and therefore it is limited to description of the laser beam refraction and collisional absorption. Recently, we developed a novel approach to hydrodynamic modeling that relies on the Paraxial Complex Geometrical Optics (PCGO) [25, 26] to describe the laser propagation and intensity in plasma by using stochastically distributed Gaussian optical beamlets. It is coupled to a reduced hot electron transport model based on the Continuous Slowing Down (CSD) approximation [27] adapted to two-dimensional, transversally Gaussian beams with exponential energy distribution. The hot electrons are created in plasma due to the resonant absorption (RA), SRS and TPD according to simplified models based on theoretical calculations and scaling laws from PIC simulations, relating the hot electron fluxes, temperatures, angular dispersion and direction with laser intensity of PCGO beamlets [28].

This model is implemented in the radiation hydrodynamics code and is resolved inline. The model performance is confirmed by comparison with the results of laser absorption in the OMEGA [29] and PALS [30] experiments. Here, we present the first results of testing this model for the SI HiPER target decribed in Sec. 2. A spherical shell of 211 μm thickness of a cryogenic DT is compressed by 10.7 ns laser beams at 60 TW peak power. An intense laser spike with 200 ps rise time is launched at 10 ns, reaching a total peak power of 260 TW and lasting for 300 ps with the intensity of 7 PW/cm^2. We account for the delay between the spike launch time and hot electron creation [18] by activating the nonlinear interaction at 10.2 ns. The model predicts average instantaneous laser power converted into the inward propagating electrons around 2.5% for RA, 5.5% for SRS and 2.2% for TPD. This can be compared with the collisional absorption of $\sim$ 30%. Average hot electron temperatures during the laser spike are of 41 keV for SRS, 98 keV for TPD and $5-7$ keV for RA. Energy deposited by hot electrons generated by SRS and TPD are illustrated in figure 8. The SRS (panel a) is the dominant preheating mechanism for two main reasons. First, the flux of SRS hot electrons is higher and they are more directional that TPD-generated hot electrons. Secondly, the TPD-generated hot electrons (panel b) that penetrate beyond the dense shell are of higher energy than SRS-generated hot electrons, and thus do not slow down as much in the hot spot. In the shell, this trend is much less significant. Hot electrons from SRS and TPD produce almost similar preheat, despite the lower TPD flux, owing to the high density of the imploding shell.

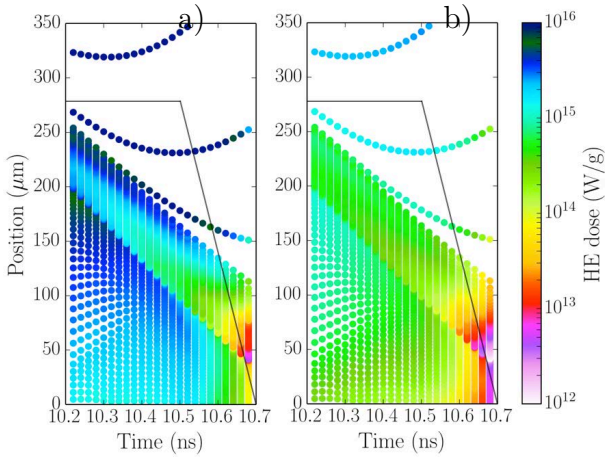

Figure 8. Dose deposition rate of hot electrons generated by SRS (a) and TPD (b) during the laser spike, as a function of time and depth into the target. The outer and inner imploding shell interfaces are visible as ruptures in the dose map. Each dot represents the barycenter of a Lagrangian mesh cell.

Two pre-heating effects need to be discussed. First, preheating of the shell increases the shock pressure by 35%, decreases the shock strength by 8% and shifts the time of peak neutron production by $\sim$ 31 ps. This time delay is due to expansion of the

preheated shell, which increases the time of shock propagation through the shell. This delay is highly significant when compared to the temporal window of 30 ps given for the shock arrival to the target center. The enhanced shock pressure also implies that less laser energy would be required to achieve a given shock pressure in agreement with the shock amplification analysis presented in Sec. 2. Furthermore, preheating of the cold shell is slow and occurs late in the implosion of the target, so that the final fuel assembly is not degraded and the thermonuclear gain of the target is unaffected.

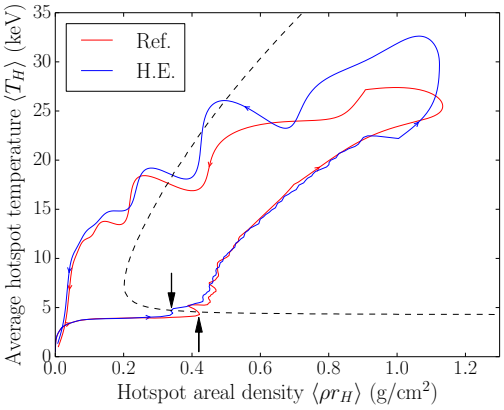

Figure 9. Thermodynamic path of the hot spot – dependence of the average temperature $\langle T_H \rangle$ on the areal density $\langle \rho r_0 \rangle$ – for the case without (solid red line) and with hot electrons (solid blue line). The black dashed line is the isobaric ignition curve [4]. Black arrows indicate the point at which fusion reactions begin.

Secondly, the most energetic electrons generated by SRS and TPD penetrate through the dense shell. Those of lower temperature (SRS) deposit a fraction of energy in the hot spot, elevating its pressure gradually at almost constant density. At the end of the laser spike, before convergence, the hot spot pressure is increased by 30%. The enhanced shock then reaches the hot spot and raises its pressure more rapidly. Consequently, fusion reactions start at a lower areal density of 0.34 compared to 0.42 g/cm^2 in the simulation without hot electrons, as indicated by black arrows in the thermodynamic path of the hot spot shown in figure 9. Therefore, the target central zone preheat by hot electrons could be beneficial for the SI scheme, as it lowers the energy required for ignition. The velocity of shock entering in hot spot is about 600 km/s, which is consistent with the analytical estimates presented in figure 2a. These results demonstrate the progress in understanding intricate physics of Shock Ignition and necessity of integrated simulations and experiments.

5. Conclusions

Shock Ignition approach offers a promising path to inertial confinement energy production as it lowers the technological requirements and provides a better control of

the implosion and ignition processes. In turn, it implies a more complicated physics involving nonlinear laser plasma interactions, understanding and control of the hot electron transport and energy deposition and overall implosion and ignition process. One of the strongest challenges of SI related to generation of strong ablation pressures exceeding 300 Mbar is demonstrated in recent experiments [8, 18] in good agreement with theoretical models. This opens way for further optimization of the target design and future experiments in full scale on the megajoule facilities NIF and LMJ.

Acknowledgments

This work was performed within the EUROfusion Consortium and has received funding from the EU's Horizon 2020 research and innovation programme, grant 633053. The support from the French National Agency of Research, projects ANR-12-BS04-0006-04 and ANR-10-IDEX-03-02, is also acknowledged.

References

[1] Lindl J. et al. 2014 *Phys. Plasmas* **21** 020501
[2] Shcherbakov V. A. 1983 *Sov. J. Plasma Phys.* **9**, 240
[3] Betti R. et al. 2007 *Phys. Rev. Lett.* **98** 155001
[4] Ribeyre X. et al. 2009 *Plasma Phys. Control. Fusion* **51** 015013
[5] Atzeni S. et al. 2014 *Nuclear Fusion* **54** 054008
[6] Batani D. et al. 2014 *Nuclear Fusion* **54** 054009
[7] http://www.hiper-laser.org/
[8] Nora R. et al. 2015 *Phys. Rev. Lett.* **114** 045001
[9] Guderley V. G. 1942 *Luftfahrtforschung* **19**, 302
[10] Ribeyre X. et al. 2011 *Phys. Plasmas* **18** 102702
[11] Vallet A. et al. 2013 *Phys. Plasmas* **20** 082702
[12] Vallet A. 2014 *Ph.D. thesis* University of Bordeaux
[13] Whitham G. B. 1958 *Journ. Fluid Mech.* **4**, 337
[14] Klimo O. et al 2010 *Plasma Phys. Control. Fusion* **52** 055013
[15] Klimo O. et al 2013 *Plasma Phys. Control. Fusion* **55** 095002
[16] Riconda C. et al 2011 *Phys. Plasmas* **18** 092701
[17] Klimo O. et al 2014 *Plasma Phys. Control. Fusion* **56** 055010
[18] Theobald W. et al 2015 *Phys. Plasmas* **22** 056310
[19] Betti R. et al 2008 *J. Phys.: Conf. Ser.* **112** 022024
[20] Gus'kov S. et al 2012 *Phys. Rev. Lett.* **109** 255004
[21] Ribeyre X. et al. 2013 *Phys. Plasmas* **20** 062705
[22] Fox T. E. et al. 2013 *Phys. Plasmas* **20** 122707
[23] Nicolaï Ph. et al. 2014 *Phys. Rev. E* **89** 033107
[24] Breil J. et al 2011 *Comput. & Fluids* **46** 161
[25] Kravtsov Y. A., Berczynski P. 2007 *Studia Geophysica et Geodaetica* **51** 1
[26] Colaïtis A. et al 2014 *Phys. Rev. E* **89** 033101
[27] Li C. K., Petrasso R. D. 2004 *Phys. Rev. E* **70** 067401
[28] Colaïtis A. et al 2015 *Phys. Rev. Lett.* submitted
[29] Boehly T. et al 1997 *Optics Communications* **133** 495
[30] Jungwirth K. et al 2001 *Phys. Plasmas* **8** 2495